

Determination of charge-compensated C_{3v} (II) centers for Er^{3+} ions in CdF_2 and CaF_2 crystals

Rui-Peng Chai(柴瑞鹏), Dan-Hui Hao(郝丹辉), Dang-Li Gao(高当丽), and Qing Pang(庞庆)

Citation: Chin. Phys. B, 2021, 30 (**3**): 037601. DOI: 10.1088/1674-1056/abc3b0
Journal homepage: http://cpb.iphy.ac.cn; http://iopscience.iop.org/cpb

What follows is a list of articles you may be interested in

Random crystal field effect on hysteresis loops and compensation behavior of mixed spin-(1,3/2) Ising system

K Htoutou, Y Benhouria, A Oubelkacem, R Ahl laamara, L B Drissi
Chin. Phys. B, 2017, 26 (**12**): 127501. DOI: 10.1088/1674-1056/26/12/127501

Exact solutions of an Ising spin chain with a spin-1 impurity

Xuchu Huang(黄旭初)
Chin. Phys. B, 2017, 26 (**3**): 037501. DOI: 10.1088/1674-1056/26/3/037501

Covalent bonding and *J-J* mixing effects on the EPR parameters of Er^{3+} ions in GaN crystal

Rui-Peng Chai(柴瑞鹏), Long Li(李隆), Liang Liang(梁良), Qing Pang(庞庆)
Chin. Phys. B, 2016, 25 (**7**): 077601. DOI: 10.1088/1674-1056/25/7/077601

An electron spin resonance study of Eu doping effect in $La_{4/3}Sr_{5/3}Mn_2O_7$ single crystal

He Li-Min, Ji Yu, Wu Hong-Ye, Xu Bao, Sun Yun-Bin, Zhang Xue-Feng, Lu Yi, Zhao Jian-Jun
Chin. Phys. B, 2014, 23 (**7**): 077601. DOI: 10.1088/1674-1056/23/7/077601

Abnormal magnetic behaviors induced by the antisite phase boundary in La_2NiMnO_6

Zhao Yue-Lei, Chai Yi-Sheng, Pan Li-Qing, Sun Young
Chin. Phys. B, 2013, 22 (**8**): 087601. DOI: 10.1088/1674-1056/22/8/087601

Determination of charge-compensated C_{3v} (II) centers for Er^{3+} ions in CdF_2 and CaF_2 crystals*

Rui-Peng Chai(柴瑞鹏)[1,†], Dan-Hui Hao(郝丹辉)[2], Dang-Li Gao(高当丽)[1], and Qing Pang(庞庆)[1]

[1] College of Science, Xi'an University of Architecture and Technology, Xi'an 710055, China
[2] Xi'an University of Architecture and Technology Huaqing College, Xi'an 710043, China

(Received 26 August 2020; revised manuscript received 21 October 2020; accepted manuscript online 22 October 2020)

A unified theoretical method is established to determine the charge-compensated C_{3v} (II) centers of Er^{3+} ions in CdF_2 and CaF_2 crystals by simulating the electron paramagnetic resonance (EPR) parameters and Stark energy levels. The potential (Er^{3+}–F^-–O_4^{2-}) and (Er^{3+}–F_7^-–O^{2-}) structures for the C_{3v} (II) centers of Er^{3+} ions in CdF_2 and CaF_2 crystals are checked by diagonalizing 364×364 complete energy matrices in the scheme of superposition model. Our studies indicate that the C_{3v} (II) centers of Er^{3+} ions in CdF_2 and CaF_2 may be ascribed to the local (Er^{3+}–F^-–O_4^{2-}) structure, where the upper ligand ion F^- undergoes an off-center displacement by $\Delta Z \approx 0.3$ Å for CdF_2 and $\Delta Z \approx 0.29$ Å for the CaF_2 along the C_3 axis. Meanwhile, a local compressed distortion of the $(ErFO_4)^{6-}$ cluster is expected to be $\Delta R \approx 0.07$ Å for CdF_2:Er^{3+} and $\Delta R \approx 0.079$ Å for CaF_2:Er^{3+}. The considerable g-factor anisotropy for Er^{3+} ions in each of both crystals is explained reasonably by the obtained local parameters. Furthermore, our studies show that a stronger covalent effect exists in the C_{3v} (II) center for Er^{3+} in CaF_2 or CaF_2, which may be due to the stronger electrostatic interaction and closer distance between the central Er^{3+} ion and ligand O^{2-} with the (Er^{3+}–F^-–O_4^{2-}) structure.

Keywords: EPR parameters, distorted local structure, covalent effect, optical properties

PACS: 76.30.–v, 75.10.Dg, 31.15.–p, 76.30.Kg **DOI:** 10.1088/1674-1056/abc3b0

1. Introduction

The metal difluorides with the formula MF_2 (M = Ca, Cd, Sr, Ba) can be used as ideal laser media, scintillators, and other optoelectronic materials, due to the excellent optical and electronic properties when activated with trivalent rare-earth ions.[1–13] Weakly interacting dopants with rare-earth ions are favourable for the possibility of production of the compact laser.[10–13] In particular, the case of Er^{3+} is of considerable interest,[14–21] since it has been found that the visible and infrared photoluminescence spectra of Er^{3+} ions with low concentration in MF_2-type fluorides are closely related to the different charge compensation centers, mainly resulting from the modification of local site symmetry and local lattice distortion.

As is well known, the MF_2-type fluorides each possess a cubic structure with the space group $Fm\bar{3}m$, and each unit cell has four formula units with twelve ions.[22] As a rule, the divalent metal ions occupy the center of cube coordinated with eight F^- ions at the vertices. When trivalent rare-earth ions enter into the MF_2-type fluorides, the trivalent magnetic impurity ions will be expected to substitute for the divalent M^{2+} ions, forming various defect sites, which are associated with the charge compensation for local charge neutrality.[23–26] In the past several decades, the electron paramagnetic resonance (EPR) as a useful tool has been widely employed to identify the defect sites of paramagnetic ions.[27–30] For instance, the five different EPR spectra of Er^{3+} in CaF_2 have been reported by Ranon and Low, which are associated with cubic or tetragonal or trigonal point symmetry.[31] Subsequently, both of C_{3v} local symmetry sites were also observed by Ensign and Byer through using correlated EPR and optical spectra for Er^{3+} in CdF_2.[32] Meanwhile, combining with the results of site-selective laser spectroscopy, some charge compensation centers have been identified, unambiguously.[33–37] For the case of Er^{3+} ions in CdF_2 and in CaF_2, it is found that the C_{4v} symmetry site arises from the charge compensation in which an F^- ion is located at the interstitial position of nearest-neighbor along the [100] axis of the cube.[35] As to the C_{3v} symmetry sites, in contrast to the single trigonal Er^{3+}center (L center) in BaF_2:Er^{3+} and (J center) in SrF_2:Er^{3+}, respectively,[36,37] there are two Er^{3+}centers identified by EPR technique for Er^{3+} ions in CaF_2 and CdF_2 crystals, one of which is designated to C_{3v} (I) center which is attributed to an interstitial fluorine ion F^- compensating for the exceeded charge along the [111] direction of crystal axis. However, differing from the C_{3v} (I) center, the other trigonal Er^{3+} site, denoted as C_{3v} (II) center, displays the larger g-factor anisotropy for each of CaF_2 and CdF_2 crystals, which is usually ascribed to the O^{2-} ions substituted for the fluorine ions at the nearest-neighbor sites of the Er^{3+} ions along the same [111] direction of cube.[31,32] However, there are some uncertainties for the identification of the charge compensators for the C_{3v} (II) centers in CaF_2 and

*Project supported by the National Natural Science Foundation of China (Grant No. 1170513), the Natural Science Foundation of Shaanxi Province, China (Grant No. Z20200051), the Foundation of the Education Department of Shaanxi Provincial Government, China (Grant No. 16JK1461), and the Scientific Research Foundation of Xi'an University of Architecture and Technology, China (Grant No. QN1729).

†Corresponding author. E-mail: chairuipeng2005@163.com

© 2021 Chinese Physical Society and IOP Publishing Ltd

CdF_2. For instance, Ranon and Low suggested that the EPR spectrum of C_{3v} (II) center in CaF_2 may be associated with a substitutional O^{2-} ion occupied at a vertex of cube surrounding the central ions, thus forming a distorted cubic structure (Er^{3+}–F_7^-–O^{2-}).[31] In comparison with the electron nuclear double resonance (ENDOR) studies of the isomorphic Yb^{3+} ions and Ce^{3+} ions in CaF_2,[38–40] Ensign and Byer reckoned that the C_{3v} (II) centers for Er^{3+} ions in CdF_2 and CaF_2 perhaps possess the (Er^{3+}–F^-–O_4^{2-}) structure, which is coordinated by three substitutional O^{2-} ions and three F^- vacancies as the nearest neighbor of the central Er^{3+} ions, forming a five-ligand $(ErFO_4)^{6-}$ cluster for the Er^{3+}-doped systems under study.[32] So far, the charge compensation mechanism for the C_{3v} (II) centers of Er^{3+} ions in CaF_2 and CdF_2 has not been confirmed, although the interstitial fluoride charge compensations of Er^{3+} doped in homotypical BaF_2 and SrF_2 crystals have been reasonably explained, and the corresponding EPR parameters related to the defect structure have been studied in the last few years by Li *et al.*[41]

The main goal of the present work is to establish the correlation between the EPR parameters and local defect structures of Er^{3+} ions in CaF_2 and CdF_2 crystals. Both of the distorted local models based on the (Er^{3+}–F^-–O_4^{2-}) and (Er^{3+}–F_7^-–O^{2-}) structures are presented to identify the potential charge compensation for C_{3v} (II) centers of Er^{3+} ions in CaF_2 and CdF_2 crystals. Unlike the method in which used is the least-squares fitting of the optical data used by Chehaidar and Hirsch,[24] the EPR parameters and Stark energy levels are simulated simultaneously by diagonalizing the 364×364 complete energy matrices for a $4f^{11}$ configuration ion in trigonal ligand-field in the scheme of superposition model. Based on the present theoretical method, the most probable charge compensation figure is identified, and the displacement of compensators away from the central ions compared with regular cubic structure is evaluated for C_{3v} (II) centers of Er^{3+} ions in CaF_2 and CdF_2. Moreover, the considerable g-factor anisotropy for C_{3v} (II) centers of Er^{3+} ions in each of CaF_2 and CdF_2 is explained reasonably, and the dependence of EPR parameters on local distortion parameter ΔZ is analyzed.

2. Theoretical methods

In general, the perturbation Hamiltonian for a $4f^{11}$ configuration ion Er^{3+} in a trigonal crystal-field can be expressed as[42–44]

$$\begin{aligned}\hat{H} =& \sum_{k=2,4,6} F^k f_k + \zeta_{4f}\sum_i \boldsymbol{l}_i\cdot\boldsymbol{s}_i + \alpha L(L+1)\\ &+\beta G(G_2)+\gamma G(R_7)+\sum_{k=0,2,4} M^k m_k\\ &+\sum_{k=2,4,6} P^k p_k + \sum_{\substack{k=2\\k\neq5}}^{8} t_k T^k + \sum_{k,q,i} B_q^k C_q^k(i),\end{aligned} \tag{1}$$

where the preceding eight terms on the right-hand side indicate the spherically symmetric free ion parts, and the last term represents the crystal-field potential function. The operators and parameters of Eq. (1) are written and defined according to traditional practice.[27–30] The crystal-field Hamiltonian with the C_{3v} site symmetry may be expanded as

$$\begin{aligned}\hat{H}_{\rm trig} =& B_0^2C_0^2+B_0^4C_0^4+B_0^6C_0^6+B_3^4(C_{-3}^4-C_3^4)\\ &+B_3^6(C_{-3}^6-C_3^6)+B_6^6(C_{-6}^6+C_6^6),\end{aligned} \tag{2}$$

where the C_q^k and B_q^k denote the normalised tensor operators and the corresponding crystal-field parameters, respectively. According to the scheme of the superposition model developed by Newman and Ng,[45,46] the crystal-field parameters B_q^k associated with the coordinates of ligand ions around the central ion may be expressed as

$$B_q^k = \sum_i a_k\bar{A}_k(R_0)\left(\frac{R_0}{R_i}\right)^{t_k} g_{k,q}(\theta_i,\phi_i), \tag{3}$$

where the $\bar{A}_k(R_0)$ and t_k denote the intrinsic crystal-field parameter and the power law exponent of rank k, respectively; R_0 is the reference distance, and the R_i represent the distance between the i-th ligand and the central Er^{3+} ion. The conventional power law exponents $t_2=3$, $t_4=4$, and $t_6=10$ will be employed in our calculations. It is noticed that the coefficients a_k ($a_2=2$, $a_4=8$, $a_6=16$) are associated with the transformation of the intrinsic parameters $\bar{A}_k(R_0)$ and $\bar{B}_k(R_0)$ in a straightforward manner.[46]

When an external magnetic field is applied, besides the perturbation Hamiltonian listed in Eq. (1), an extra Zeeman operator is required. In the intermediate coupling scheme with $|\gamma SLJM_J\rangle$ basis, the matrix elements of the Zeeman interaction $\hat{H}_{\rm Zee}$ may be expressed as[44]

$$\begin{aligned}&\left(f^N\gamma SLJM_J\left|\sum_i\beta\boldsymbol{H}\cdot(k\boldsymbol{l}_i+g_s\boldsymbol{s}_i)_q^{(1)}\right|f^N\gamma'S'L'J'M_J'\right)\\ &=(-1)^{J-M_J}\beta H\begin{pmatrix}J & 1 & J'\\ -M_J & q & M_J'\end{pmatrix}\\ &\times\left(\gamma SLJ\,\|kL+g_sS\|\,\gamma'S'L'J'\right),\end{aligned} \tag{4}$$

where

$$\begin{aligned}&\left(\gamma SLJ\,\|kL+g_sS\|\,\gamma'S'L'J'\right)\\ &=\delta(S,S')\delta(L,L')\left\{[J][J']\right\}^{1/2}\left\{k(-1)^{S'+L'+J+1}\begin{Bmatrix}J & 1 & J'\\ L' & S & L\end{Bmatrix}\right.\\ &\times[L(L+1)(2L+1)]^{1/2}+g_s(-1)^{S+L+J'+1}\\ &\left.\times\begin{Bmatrix}J & 1 & J'\\ S' & L & S\end{Bmatrix}[S(S+1)(2S+1)]^{1/2}\right\}.\end{aligned} \tag{5}$$

Note that the magnetic hyperfine interaction $\hat{H}_{\rm HF}$ will replace the Zeeman operator, when the EPR hyperfine structural parameters ($A_\parallel$, $A_\perp$) are studied. In contrast to the Zeeman operator, the magnetic hyperfine interaction $\hat{H}_{\rm HF}$ arises from the

interaction between the electrons and nucleus and may be written as

$$\hat{H}_{\rm HF} = \frac{2\beta\beta_N\mu_N}{I}\sum_i \frac{\boldsymbol{N}_i\cdot\boldsymbol{I}}{r_i^3}, \tag{6}$$

where $\boldsymbol{N}_i = \boldsymbol{l}_i - \sqrt{10}(\boldsymbol{sC}^2)_i^{(1)}$, β and β_N denote the Bohr magneton and the nuclear magneton, respectively; μ_N is the value of the nuclear magnetic moment in the unit of nuclear magneton, and I represents the nuclear spin ($I = 7/2$ for the $^{167}Er^{3+}$ isotope). The basic matrix elements of the second part of $\boldsymbol{N}_i$ in the same coupling scheme may be expressed as

$$\begin{aligned}&\left(f^N\gamma SLJM_J\left|\sum_i(\boldsymbol{s}_i\boldsymbol{C}_i^2)_q^{(1)}\right|f^N\gamma'S'L'J'M_J'\right)\\ &= (-1)^{J-M_J}\begin{pmatrix} J & 1 & J'\\ -M_J & q & M_J'\end{pmatrix}\\ &\quad\times\left(f^N\gamma SLJ\left\|\sum_i(\boldsymbol{sC}^2)_i^{(1)}\right\|f^N\gamma'S'L'J'\right),\end{aligned} \tag{7}$$

where the sum i runs over all the unfilled electrons. The reduced matrix elements of the generalized tensor on the extreme right side of Eq. (7) can be further reduced to

$$\begin{aligned}&\left(f^N\gamma SLJ\left\|\sum_i(\boldsymbol{sC}^2)_i^{(1)}\right\|f^N\gamma'S'L'J'\right)\\ &= -\sqrt{\frac{42}{5}}N\left\{[J][J'][L][L'][S][S']\right\}^{1/2}\begin{Bmatrix} S & S' & 1\\ L & L' & 2\\ J & J' & 1\end{Bmatrix}\\ &\quad\times\sum_{\bar\gamma\bar L\bar S}\left(\gamma LS\{|\bar\gamma\bar L\bar S l\right)\left(\gamma'L'S'\{|\bar\gamma\bar L\bar S l\right)(-1)^{\bar L+\bar S+L+S+s}\\ &\quad\times\begin{Bmatrix} S & 1 & S'\\ s & \bar S & s\end{Bmatrix}\begin{Bmatrix} L & 2 & L'\\ l & \bar L & l\end{Bmatrix}.\end{aligned} \tag{8}$$

For the sake of saving space, the abbreviation $[Y] = 2Y+1$ is used and valid only when there is a single symbol enclosed within the square brackets in Eq. (8). With simple manipulation of transformation, the relations between the components of these vector operators in the Cartesian coordinates systems and the components of the corresponding tensor operators may be written as follows:

$$T_x = (1/\sqrt{2})(T_{-1}^{(1)} - T_1^{(1)}), \tag{9}$$

$$T_y = \frac{\mathrm{i}}{\sqrt{2}}(T_{-1}^{(1)} + T_1^{(1)}), \tag{10}$$

$$T_z = T_0^{(1)}, \tag{11}$$

where T represents the first-order tensor operator acting as orbital angular momentum L, spin angular momentum S or the generalized first-order tensor $\sum_i(\boldsymbol{sC}^2)_i^{(1)}$. Up to now, the EPR parameters of a $4f^{11}$ configuration ion Er^{3+} in the trigonal ligand-field can be analysed by using the effective spin Hamiltonian[47]

$$\hat{H}_S = \beta H_z g_\parallel S_z + \beta g_\perp(H_xS_x + H_yS_y) + A_\parallel I_zS_z + A_\perp(S_xI_x + S_yI_y), \tag{12}$$

where effective $S = 1/2$ is taken. The constants required for following calculations are $\langle r^{-3}\rangle = 10.6$ a.u. and $\mu_N = -0.5647$ for the $^{167}Er^{3+}$ isotope.[29] The correlation between the EPR parameters and the actual Hamiltonian is established by completing the energy matrices.

3. Calculations and discussion

As is well known, the ground $^4I_{15/2}$ multiplet for a $4f^{11}$ configuration ion Er^{3+} in a cubic ligand-field will be split into three quartets Γ_8 and both doublets Γ_6 and Γ_7, of which the three quartets Γ_8 may be further split into six doublets under the lower trigonal site symmetry. For the C_{3v} (II) centers of Er^{3+} ions in CaF_2 and CdF_2 crystals, the lowest Kramers' doublet Γ_7 can be determined by the diagrams by Lea *et al.*[48] and or the method reported in our earlier paper.[49] In the present work, firstly, the optical spectra of Er^{3+} ions in CaF_2 and CdF_2 crystals in cubic symmetry are simulated by diagonalizing 364×364 complete energy matrices.[25] The fourth-order and sixth-order intrinsic parameters $\bar A_4 \approx 76.6$ cm^{-1}, $\bar A_6 \approx 22.9$ cm^{-1} for CaF_2:Er^{3+} system, and $\bar A_4 \approx 80.6$ cm^{-1}, $\bar A_6 \approx 24.3$ cm^{-1} for CdF_2:Er^{3+} system are obtained, respectively, which will be employed in the next studies for the C_{3v} (II) centers in CaF_2 and CdF_2. Secondly, based on the suggested (Er^{3+}–F^-–O_4^{2-}) or (Er^{3+}–F_7^-–O^{2-}) structure for C_{3v} (II) centers in CaF_2 and CdF_2, the distorted local models are proposed and plotted in Fig. 1, where the parameter ΔZ corresponds to the displacement of the upper ligand ion, viz., F^- for the (Er^{3+}–F^-–O_4^{2-}) structure and O^{2-} for the (Er^{3+}–F_7^-–O^{2-}) structure along the C_3 axis. The changes of the remaining ligand ions with equivalent charge and location in the nearest neighbor of $Er^{3+}$are described by the parameter ΔR compared with the scenario of the cubic structures. Thus, the lengths of the Er^{3+}–F^- bond and Er^{3+}–O^{2-} bond for the (Er^{3+}–F^-–O_4^{2-}) structure, or the lengths of the reversed Er^{3+}–O^{2-} bond and Er^{3+}–F^- bond for the (Er^{3+}–F_7^-–O^{2-}) structure, can be expressed, respectively, as

$$R_1 = R_0 - \Delta Z, \quad R_2 = R_0 - \Delta R, \tag{13}$$

where $R_0 = 2.333$ Å and $R_0 = 2.366$ Å denote the Cd^{2+}–F^- bond length and Ca^{2+}–F^- bond length for the host CdF_2 and CaF_2, respectively. In our calculations, in order to reduce the number of adjustable parameters, the well-fitting free-ion parameters of Er^{3+} ions doped in LaF_3 are used,[41] because a number of studies have proved that the slight variation of free-ion parameters hardly affects the Stark splitting or the EPR parameters, merely disturbing the centroid of high manifolds.[27–30] By simulating the Stark energy levels and EPR parameters of Er^{3+} ions in CaF_2 and CdF_2 with C_{3v} (II) centers based on the above distorted models, we determine the values of other intrinsic parameters: $A_2(F^-) \approx 695.0$ cm^{-1}, $A_4'(O^{2-}) \approx 120.4$ cm^{-1},

$A_6'(O^{2-}) \approx 29.3\ cm^{-1}$ for $CdF_2:Er^{3+}$; $A_2(F^-) \approx 1265.0\ cm^{-1}$, $A_4'(O^{2-}) \approx 115.4\ cm^{-1}$, $A_6'(O^{2-}) \approx 22.1\ cm^{-1}$ for $CaF_2:Er^{3+}$ with the (Er^{3+}–F^-–O_4^{2-}) structure; $A_2(F^-) \approx 400\ cm^{-1}$, $A_2'(O^{2-}) \approx 1000\ cm^{-1}$, $A_4'(O^{2-}) \approx 185.6\ cm^{-1}$, $A_6'(O^{2-}) \approx 18.9\ cm^{-1}$ with the (Er^{3+}–F_7^-–O^{2-}) structure for $CaF_2:Er^{3+}$ system. The obtained crystal-field parameters and the Stark energy levels are tabulated in the following Table 1 and Table 2, respectively. The comparisons between the calculated EPR parameters and the experimental values are given in Table 3.

Table 1. The crystal-field parameters for Er^{3+} ions in CdF_2 and CaF_2 crystals, in units of cm^{-1}.

Parameter	$CdF_2:Er^{3+}$		$CaF_2:Er^{3+}$		
Symmetry	O_h	C_{3v} (II)[a]	O_h	C_{3v} (II)[a]	C_{3v} (II)[b]
B_{20}	0	759.2	0	1419.2	1617.0
B_{40}	1337.4	1511.2	1271	1480.0	2436.2
B_{43}	–1598.5	–1433.3	–1519.1	–1402.9	–1519.2
B_{60}	1228.8	1120.6	1158.0	900.0	1199.9
B_{63}	742	606.6	699	473.8	699.2
B_{66}	778.2	636.2	733.3	497.0	733.3

[a] Crystal-field parameters based on the (Er^{3+}–F^-–O_4^{2-}) structure.
[b] Crystal-field parameters based on the (Er^{3+}–F_7^-–O^{2-}) structure.

Table 2. The calculated and experimental Stark energy levels of $^4I_{15/2}$ states for C_{3v} (II) centers of Er^{3+} ions in CdF_2 and CaF_2 crystals. All values are in units of cm^{-1}.

Stark levels No.	$CdF_2:Er^{3+}$		$CaF_2:Er^{3+}$			
	E_{exp} [32]	E_{cal}[a]	E_{exp} [24]	E_{exp} [36]	$E_{cal}^{a)}$	$E_{cal}^{b)}$
Z_1	0.0	0.0	0.0	0.0	0.0	0.0
Z_2	65.5	68.4	48.99	50.3	53.2	61.4
Z_3	93.4	87.1	97.47	99.8	99.0	96.8
Z_4	135.7	112.0	198.45	199.0	183.7	197.3
Z_5	494.6	489.4	425.88	428.5	426.0	536.5
Z_6	522.2	521.0	439.38	442.5	448.1	563.6
Z_7	554.6	554.2	455.87	457.5	458.2	590.0
Z_8	701.4	705.9	744.27	750.5	749.0	990.2

[a] Calculated results based on the (Er^{3+}–F^-–O_4^{2-}) structure.
[b] Calculated results based on the (Er^{3+}–F_7^-–O^{2-}) structure.

Table 3. The calculated and observed EPR parameters for C_{3v} (II) centers of Er^{3+} ions in CdF_2 and CaF_2 crystals, the hyperfine parameters are in units of $10^{-4}\ cm^{-1}$.

$CdF_2:Er^{3+}$	ΔZ	ΔR	k	$g_\parallel$	$g_\perp$	g_{av}	$A_\parallel$	$A_\perp$
Cub.								
Cal.	–	–	1.0	6.8202	6.8202	6.8202		
Cal.	–	–	0.986	6.757	6.757	6.757		
Exp.[32]				**6.759**	**6.759**	**6.759**		
C_{3v} (II)								
Cal.	–0.30	0.07	1.0	2.9618	8.5975	6.7189	105.6	311.45
Cal.	–0.30	0.07	0.955	2.8747	8.3406	6.5186	100.85	297.44
Exp.[32]				**2.875**	**8.334**	**6.514**		
$CaF_2:Er^{3+}$								
Cub.								
Cal.	–	–	1.0	6.8185	6.8185	6.8185		
Cal.	–	–	0.992	6.783	6.783	6.783		
Exp.[31]				**6.785**	**6.785**	**6.785**		
C_{3v} (II)								
Cal.[a]	0.07	0.0	1.0	2.1734	8.883	6.646		
Cal.[b]	–0.29	0.079	0.97	2.2073	8.8339	6.625	78.34	319.93
Exp.[31]				**2.206**	**8.843**	**6.631**	**77±6**	**305±6**

[a] Calculated results based on the (Er^{3+}–F_7^-–O^{2-}) structure.
[b] Calculated results based on the (Er^{3+}–F^-–O_4^{2-}) structure.

By comparison, we find that the EPR parameters and Stark energy levels for the C_{3v} (II) centers of Er^{3+} ions in CdF_2 and CaF_2 can well accord with the experimental values if the (Er^{3+}–F^-–O_4^{2-}) structure is adopted, where the parameters $\Delta Z \approx -0.3$ Å, $\Delta R \approx 0.07$ Å for CdF_2:Er^{3+}, and $\Delta Z \approx -0.29$ Å, $\Delta R \approx 0.079$ Å for CaF_2:Er^{3+} are obtained, respectively. In contrast to the case of the (Er^{3+}–F^-–O_4^{2-}) structure, only the EPR g-factors and the lower four Stark energy levels of Er^{3+} in CaF_2 are in accordance with the observed values, providing that the (Er^{3+}–F_7^-–O^{2-}) structure is used. The case of CdF_2 is similar to the CaF_2 that is omitted herein. The higher four energy levels of $^4I_{15/2}$ (Z_5–Z_8) have the larger difference (more than 100 cm^{-1}) between the calculated and observed values as indicated in Table 2, even if the more intrinsic crystal-field parameters are allowed to vary freely. Furthermore, it is worth noting that the shift directions of upper ligand ions based on the above both structures are opposite to each other in order to accommodate the considerable g-factor anisotropy for the C_{3v} (II) centers. In order to clarify the potential origination, the correlation between the higher Stark energy levels of $^4I_{15/2}$ and the shift parameter ΔZ is plotted in Fig. 2, and the dependence of EPR g-factors on the parameter ΔZ is plotted in Fig. 3. From Fig. 2 we can clearly see that the Stark splitting of the energy levels $Z_7 \leftrightarrow Z_8$ is extremely sensitive to the shift parameter ΔZ whether for the (Er^{3+}–F^-–O_4^{2-}) or (Er^{3+}–F_7^-–O^{2-}) structure. In particular, the displacement of upper ligand ion ($\Delta Z > 0$) toward the central ion Er^{3+} will exponentially increase the splitting for the paired energy levels $Z_7 \leftrightarrow Z_8$. In other words, the splitting of the pair levels ($Z_7 \leftrightarrow Z_8$) can be regarded as a criterion of the shift direction of the upper ligand ion. The larger displacement ΔZ of ligand F^- from the center Er^{3+} ions with the (Er^{3+}–F^-–O_4^{2-}) structure may result in the stronger g-factor anisotropy for the C_{3v} (II) centers in CaF_2 and CaF_2.

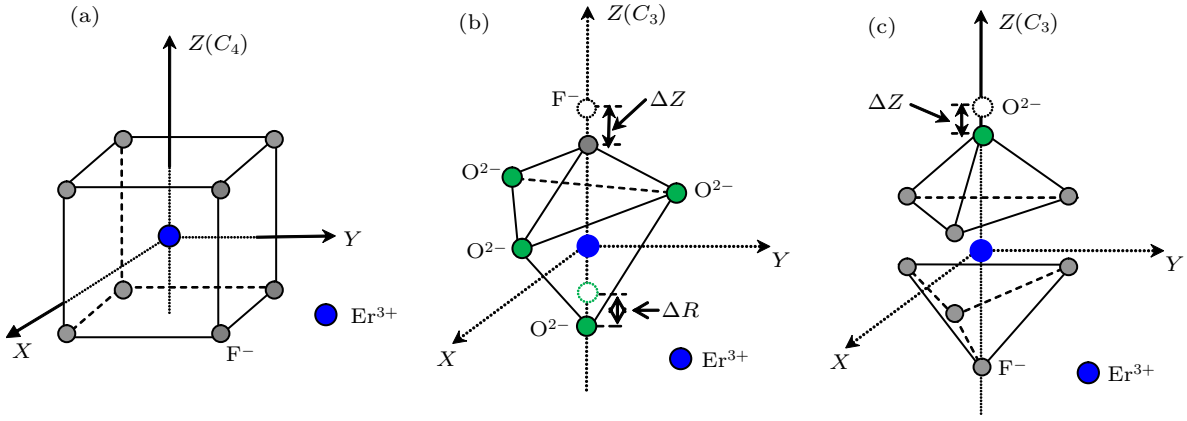


Fig. 1. The distorted local structures of Er^{3+} ions in CaF_2 and CdF_2 crystals: (a) for the cubic center without charge compensation; (b) for the C_{3v} (II) center with the (Er^{3+}–F^-–O_4^{2-}) structure; (c) for the C_{3v} (II) center with the (Er^{3+}–F_7^-–O^{2-}) structure.

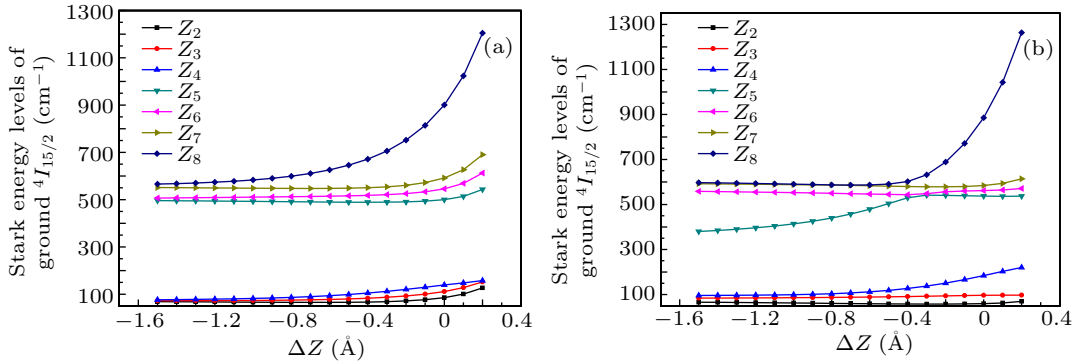


Fig. 2. Dependence of Stark energy levels (Z_2–Z_8) of $^4I_{15/2}$ on shift parameter ΔZ of Er^{3+} ions in CaF_2 for (a) (Er^{3+}–F^-–O_4^{2-}) structure and (b) (Er^{3+}–F_7^-–O^{2-}) structure.

From Fig. 3 it is shown that the closer distance ($\Delta Z > 0$) of the Er^{3+}–O^{2-} bond in the (Er^{3+}–F_7^-–O^{2-}) structure will produce stronger nephelauxetic overlap, characterised by the departure of average g-factor g_{av} from the g-value of cubic structure, than the Er^{3+}–F^- bond in the (Er^{3+}–F^-–O_4^{2-}) structure. However, the dependence for each of g-factors ($g_{\parallel}$, $g_{\perp}$, g_{av}) on the shift parameter ΔZ is analogous for both structures when ΔZ<0. In other words, the EPR g-factors almost linearly depend on the parameter ΔZ, when the upper ligand ion is faraway from the C_{3v} (II) center along the [111] axis; contrarily, Fig. 3 exhibits the presence of nonlinear dependence between the g-factors and ΔZ for both structures when $\Delta Z > 0$. To demonstrate the non-linear relation between the g-factors and the shift parameter ΔZ (> 0), the polynomial functions of g-factors can be estimated by the least squares fitting method for the Er^{3+} ions in CaF_2 with the (Er^{3+}–F^-–O_4^{2-}) structure as

follows:

$$g_{\parallel} = 43.33\Delta Z^3 - 10.38\Delta Z^2 - 0.9169\Delta Z + 2.231, \quad (14)$$

$$g_{\perp} = -15.42\Delta Z^3 + 5.40\Delta Z^2 - 0.1108\Delta Z + 8.557, \quad (15)$$

$$g_{\rm av} = 4.166\Delta Z^3 + 0.141\Delta Z^2 - 0.3796\Delta Z + 6.448, \quad (16)$$

where the maximal root-mean-squqre (RMS) deviation from the calculated values is less than 0.01. Up to now, the reason appears to be clear. The more charges of the substituted Er^{3+} ion and the ligand O^{2-} ion in the (Er^{3+}–F^-–O_4^{2-}) structure will bring about the stronger electrostatic interaction between the central Er^{3+} ion and ligand ions than the scenario at the cubic site of (Er^{3+}–F_8^-) structure without charge compensation. Since the orbit reduction factor k usually reflects the average covalent effect,[30,50] the less orbit reduction factor k with the (Er^{3+}–F^-–O_4^{2-}) structure also implies that the stronger covalent bonding effects may exist in the C_{3v} (II) centers for Er^{3+} ions in CaF_2 and CaF_2, which consists well with the calculated average g-factor $g_{\rm av}$. The less k of C_{3v} (II) center in CdF_2 means the stronger covalent bond effect than that in CaF_2 host, which may be ascribed to the less difference in ion radius between the substituted Er^{3+} ion ($r_{Er^{3+}} = 0.881$ Å) and the host ion Cd^{2+} ($r_{Cd^{2+}} = 0.97$ Å) in CdF_2 compared with the replaced Ca^{2+} ion ($r_{Ca^{2+}} = 0.99$ Å) in CaF_2 host. Moreover, the fact that the obtained parameter ΔR with the (Er^{3+}–F^-–O_4^{2-}) structure is less than the difference in ion radii between the substituted Er^{3+} ion and host ions also supports the judgment about the covalence. However, for the case of (Er^{3+}–F_7^-–O^{2-}) structure, the nominal electrovalent bond with $k = 1.0$ for C_{3v} (II) center in CaF_2 cannot account for the deviation of mean g-factor from the value of cubic center without charge compensation. It is concluded that the Stark energy levels and EPR parameters of the C_{3v} (II) centers of Er^{3+} ions in CaF_2 and CdF_2 cannot be explained reasonably by the (Er^{3+}–F_7^-–O^{2-}) structure.

In addition, the calculated hyperfine parameters of C_{3v} (II) center of Er^{3+} ions (Er^{167}, $I = 7/2$) in CaF_2 are reasonably consistent with the experimental values based on the distorted model with the (Er^{3+}–F^-–O_4^{2-}) structure. However, the breadth of the Er^{3+} EPR lines means the presence of a doublet structure for the magnetic field along the [111] direction, and the hyperfine parameters of C_{3v} (II) center of Er^{3+} ions in CdF_2 have not been reported in experiment. The calculated values of hyperfine structural parameters $A_{\parallel} = 100.85(10^{-4}\ {\rm cm}^{-1})$ and $A_{\perp} = 297.44(10^{-4}\ {\rm cm}^{-1})$ for C_{3v} (II) center in CdF_2 are obtained, which also accord well with the conventional relation between the g-tensor and A-tensor: $A_{\parallel}/g_{\parallel} \approx A_{\perp}/g_{\perp}$. Of course, considering the complexity of the local charge compensation, for the sake of clarifying the local parameters around the Er^{3+} with C_{3v} (II) centers in CdF_2 and CaF_2 crystals, a careful experimental study especially ENDOR is required.

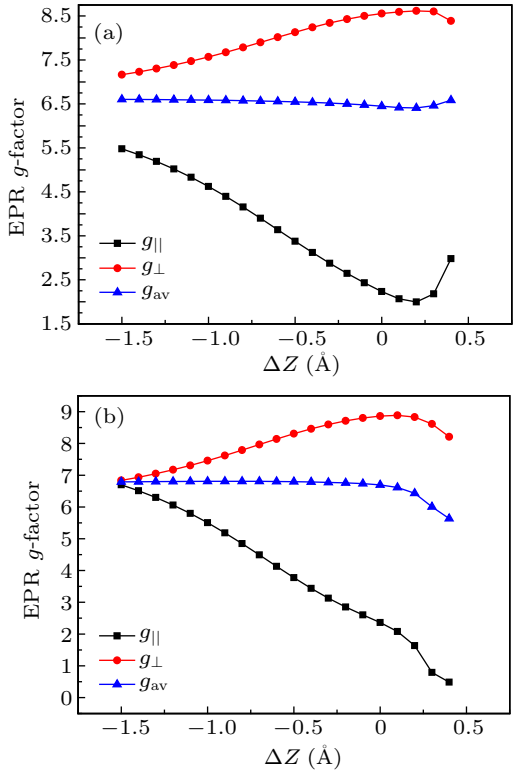


Fig. 3. The dependence of EPR g-factors on the parameter ΔZ for Er^{3+} ions in CaF_2: (a) for the (Er^{3+}–F^-–O_4^{2-}) structure and (b) for the (Er^{3+}–F_7^-–O^{2-}) structure.

4. Conclusions

The potential (Er^{3+}–F^-–O_4^{2-}) and (Er^{3+}–F_7^-–O^{2-}) structures for the C_{3v} (II) centers of Er^{3+} ions in CdF_2 and CaF_2 crystals are checked by diagonalizing 364×364 complete energy matrices in the scheme of superposition model. Our studies indicate that the C_{3v} (II) centers of Er^{3+} ions in CdF_2 and CaF_2 may be ascribed to the local (Er^{3+}–F^-–O_4^{2-}) structure, where the upper ligand ion F^- undergoes an off-center displacement $\Delta Z \approx 0.3$ Å for host CdF_2 and $\Delta Z \approx 0.29$ Å for the host CaF_2 along the C_3 axis. Meanwhile, a local compressed distortion $\Delta R \approx 0.07$ Å for CdF_2:Er^{3+} and $\Delta R \approx 0.079$ Å for CaF_2:Er^{3+} are expected. The larger g-factor anisotropy for Er^{3+} ions in each of both crystals is explained reasonably by the obtained shift parameters. Furthermore, our studies show that a stronger covalent bonding effect exists in the C_{3v} (II) center for Er^{3+} in each of CaF_2 and CdF_2, which may be due to the stronger electrostatic interaction and closer distance between the central Er^{3+} ion and ligand ion O^{2-} with the (Er^{3+}–F^-–O_4^{2-}) structure. The less difference in ion radius between the substituted Er^{3+} ion and the cation Cd^{2+} in CdF_2 may be responsible for the stronger covalence than in CaF_2 host.

References

[1] Struebing C, Chong J Y, Lee G, Zavala M, Erickson A, Ding Y, Wang C L, Diawara Y, Engles R, Wagner B and Kang Z T 2016 *Appl. Phys. Lett.* **108** 153106

[2] Jacobsohn L G, Mcpherson C L, Sprinkle K B, Yukihara E G, Devol T A and Ballato J 2011 *Appl. Phys. Lett.* **99** 113111

[3] Ivanovskikh K V, Hughes-Currie R B, Reid M F, Wells J P R, Sokolov N S and Reeves R J 2016 *J. Appl. Phys.* **119** 104305
[4] Cortelletti P, Pedroni M, Boschi F, Pin S, Ghigna P, Canton P, Vetrone F and Speghini A. 2018 *Cryst. Growth Des.* **18** 686
[5] Su F H, Chen W, Ding K and Li G H 2008 *J. Phys. Chem. A* **112** 4772
[6] Barandiarán Z and Seijo L 2015 *J. Chem. Phys.* **143** 144702
[7] Rakov N and Maciel G S 2017 *J. Appl. Phys.* **121** 113103
[8] Yang Z, Guo C F, Chen Y Q, Li L, Li T and Jeong J H 2014 *Chin. Phys. B* **23** 064212
[9] Hu T J, Cui X Y, Wang J S, Zhang J K, Li X F, Yang J H and Gao C X 2018 *Chin. Phys. B* **27** 016401
[10] Zhang F, Zhang H N, Liu D H, Liu J, Ma F K, Jiang D P, Pang S Y, Su L B and Xu J 2017 *Chin. Phys. B* **26** 024205
[11] Lopes C C, Barros V S M, Asfora V K, Yamamoto, Khoury H J and Guzzo P 2018 *J. Lumin.* **199** 266
[12] Li W W, Huang H J, Mei B C, Wang C, Liu J, Wang S Z, Jiang D P and Su L B 2020 *Ceram. Int.* **46** 19530
[13] Wang R, Yuan M H, Zhang C F, Wang H Y and Xu X J 2018 *Opt. Mater.* **79** 403
[14] Balabhadra S, Reid M F, Golovko V and Wells J P R 2020 *J. Alloys Compd.* **834** 155165
[15] Bendjedaa F, Diaf M, Boulma E, Djellab S, Guerbous L and Jouart J P 2017 *J. Alloys Compd.* **693** 48
[16] Souza W S, Domingues R O, Bueno L A, da Costa E B and Gouveia A S 2013 *J. Lumin.* **144** 87
[17] Zhang C M, Hou Z Y, Chai R T, Cheng Z Y, Xu Z H, Li C X, Huang L and Lin J 2010 *J. Phys. Chem. C* **114** 6928
[18] Ma C S, Jiao Q, Li L J, Zhou D C, Yang Z W, Song Z G and Qiu J B 2014 *Chin. Phys. B* **23** 057802
[19] Hu Y B, Qiu J B, Zhou D C, Song Z G, Yang Z W, Wang R F, Jiao Q and Zhou D L 2014 *Chin. Phys. B* **23** 024205
[20] Lian H Z, Liu J, Ye Z R and Shi C S 2004 *Chem. Phys. Lett.* **386** 291
[21] Lie L, Xie B X, Li Y Y, Zhang J J and Xu S Q 2017 *J. Lumin.* **190** 462
[22] Eftimie E L A, Avram C N, Brik M G, Chernyshev V A and Avram N M 2019 *J. Lumin.* **214** 116577
[23] Aminov L K, Gafurov M R, Kurkin I N, Malkin B Z and Rodionov A A 2018 *Phys. Solid State* **60** 912
[24] Chehaidar A and Hirsch L 2000 *Eur. Phys. J. A* **12** 79
[25] Leśniak K 1990 *J. Phys.: Condens. Matter* **2** 5563
[26] Leung A F 1973 *J. Phys. C: Solid State Phys.* **6** 2234
[27] Chai R P, Kuang X Y, Liang L and Yu G H 2015 *J. Phys. Chem. Solids* **80** 1
[28] Chai R P, Hao D H, Kuang X Y and Liang L 2015 *Spectrochim. Acta Part A* **150** 829
[29] Chai R P, Kuang X Y, Duan M L and Zhang C X 2010 *Spectrochim. Acta Part A* **77** 253
[30] Chai R P, Li L, Liang L and Pang Q 2016 *Chin. Phys. B* **25** 077601
[31] Ranon U and Low W 1963 *Phys. Rev.* **132** 1609
[32] Ensign T C and Byer N E 1973 *Phys. Rev. B* **7** 907
[33] Tallant D R and Wright J C 1975 *J. Chem. Phys.* **63** 2074
[34] Mho S and Wright J C 1984 *J. Chem. Phys.* **81** 1421
[35] Cockroft N J, Thompson D, Jones G D and Syme R W G 1987 *J. Chem. Phys.* **86** 521
[36] Cockroft N J, Jones G D and Syme R W G 1990 *J. Chem. Phys.* **92** 2166
[37] Miller M P and Wright J C 1978 *J. Chem. Phys.* **68** 1548
[38] Reddy T Rs, Davies E R, Baker J M, Chambers D N, Newman R C and Özbay B 1971 *Phys. Lett. A* **36** 231
[39] Chambers D N, Newman R C 1971 *J. Phys. C: Solid State Phys.* **4** 3015
[40] Chambers D N, Newman R C 1971 *J. Phys. C: Solid State Phys.* **5** 997
[41] Li H, Kuang X Y, Mao A J and Li C G 2013 *Spectrochim. Acta Part A.* **102** 169
[42] Carnall W T, Goodman G L, Rajnak K and Rana R S 1989 *J. Chem. Phys.* **90** 3443
[43] Liu G K and Jacquier B 2005 *Spectroscopic Properties of Rare Earths in Optical Materials* (Beijing: Tsinghua University Press and Berlin, Heidelberg: Springer-Verlag) pp. 11–37
[44] Wybourne B G 1965 *Spectroscopic Properties of Rare Earths* (New York: John Wiley & Sons, Inc.) p. 39
[45] Newman D J and Ng B 1989 *Rep. Prog. Phys.* **52** 699
[46] Newman D J and B Ng 2000 *Crystal Field Handbook* (Cambridge: Cambridge University Press) pp. 6–43
[47] Abragam A and Bleaney B 1986 *Electron Paramagnetic Resonance of Transition Ions* (New York: Dover Publications, Inc.) pp. 277–341
[48] Lea K R, Leask M J M and Wolf W P 88 1962 *J. Phys. Chem. Solids* **23** 1381
[49] Chai R P, Kuang X Y, Li C G and Zhao Y R 2011 *Chem. Phys. Lett.* **505** 65
[50] Jørgensen C K 1962 *Absorption Spectra and Chemical Bonding in Complexes* (Oxford: Pergamon Press) p. 296